Crystal structures, magnetic studies, and paramagnetic resonance of the copper trimer stacks (4-picolinium)$_2$Cu$_3$Cl$_8$, (4-picolinium)$_2$Cu$_3$Br$_8$, and (1,1,4-trimethylpiperazinium)Cu$_3$Cl$_8$

Marcus R. Bond and Roger D. Willett
Materials Science Program, Washington State University, Pullman, Washington 99164-4630

R. S. Rubins
Department of Physics, Montana State University, Bozeman, Montana 59717 and the University of Texas at Arlington, Box 19059, Arlington, Texas 76019

P. Zhou, C. E. Zaspel,* Stuart L. Hutton,† and John E. Drumheller
Department of Physics, Montana State University, Bozeman, Montana 59717
(Received 9 April 1990; revised manuscript received 2 July 1990)

Three new compounds containing planar, bibridged $Cu_3X_8^{2-}$ (X=Cl$^-$ or Br$^-$) anions have been studied. These are (1,1,4-trimethylpiperazinium)Cu$_3$Cl$_8$ (henceforth TMPC), (4-picolinium)$_2$Cu$_3$Cl$_8$ (henceforth 4-PCC), and (4-picolinium)$_2$Cu$_3$Br$_8$ (henceforth 4-PCB). The trimers form stacks parallel to the a axis (TMPC) or the c axis (4-PCC and 4-PCB) through the formation of semicoordinate Cu $\cdots$ X linkages. The powder magnetic susceptibility has been measured for TMPC in fields up to 5000 Oe and at temperatures down to 4.2 K. The individual trimers couple antiferromagnetically with an intratrimer exchange of $J/k = -33$ K, yielding a spin-$\frac{1}{2}$ ground state at low temperatures. Intrastack interactions appear to favor a ferromagnetic ground state for the stacks, with antiferromagnetic interactions between stacks. No spin frustration occurs within the stacks, in contrast to previously studied $A_2Cu_3X_8$ systems. EPR measurements at 9.2 GHz on 4-PCC are consistent with a previous magnetic study that showed that there is antiferromagnetic coupling within each trimer and weak ferromagnetic coupling between trimers. Resolved spectra were observed only at low temperatures, where measurements of the $S=\frac{1}{2}$ trimer ground state near 15 K in three mutually perpendicular crystal planes gave the principal values $g_x=2.047\pm0.001$, $g_y=2.068\pm0.002$, $g_z=2.264\pm0.001$, where z and x directions are in the ac plane, with the former making an angle of $26\pm2°$ with the c axis. Linewidth measurements in the ac plane showed three pairs of maxima and minima with peak-to-peak widths varying in one crystal from 60 to 310 G. Much broader lines were observed in 4-PCB. Unexplained $S=\frac{3}{2}$ spectra were observed below 30 K in orientations close to the c axis in 4-PCC.

I. INTRODUCTION

The magnetic properties of copper halide salts consisting of stacked copper (II) oligomers have been studied both theoretically and experimentally.[1] These compounds, consisting of pseudoplanar bibridged copper halide $Cu_nX_{2n+2}^{2-}$ oligomers, contain basic units with linear arrangements of two (I), three (II), four (III), or more copper ions. These units can aggregate in various ways to form stacks

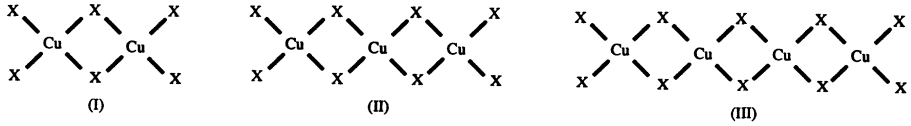

of oligomers.[2] One reason for the interest in the magnetic properties for these compounds is that the chains formed by the stacked bibridged copper halide oligomers are often isolated from other chains by nonmagnetic ions. In addition, the stacking arrangement is such that spin-frustration behavior is possible with the appropriate values of exchange coupling.[3] Consequently, these form a class of one-dimensional (1D) or pseudo-1D magnets on which experiments can be performed to test theories and approximations. The majority of these compounds contain $Cu_2X_6^{2-}$ dimers,[4] but a substantial number of copper trimers[5,6] as well as tetramers are known.[7,8] Isolated examples of oligomers with five, six, and seven copper (II) ions are also known.[9–11] The emphasis on this paper will be on a new series of trimeric salts recently synthesized.

One of the earliest studies[12] on $S=\frac{1}{2}$ trimer chains was performed on 3CuCl$_2$·2Dx, where Dx is 1,4-dioxane. The

structure of this compound consists of an unusual alternating bibridged copper chloride chain and was shown to behave magnetically as a linear antiferromagnetic chain of ferromagnetically coupled trimers. Since the ground state of the isolated ferromagnetic trimer is a quartet state, an estimate of the antiferromagnetic intertrimer exchange, J', was obtained by fitting the low-temperature susceptibility data to a model derived from Weng's[13] numerical calculation for a Heisenberg spin-$\frac{3}{2}$ chain. Another system treated as a chain of interacting trimers is $[(CH_3)_2CHNH_3]_2CuCl_4$, in which one may notice that a deviation of the data from the noninteracting trimer model calculation indicates an appreciable existence of intertrimer exchange.[14] More recently, the salts $Cu(C_4H_8SO)_4Cu_2X_6$ have been also treated as a coupled chain of trimers.[15]

The most thorough study of extended copper trimer systems has been carried out on a series of psuedo-planar trinuclear copper (II) halide salts[5] in which the most common stacking patterns observed for the trimers are schematically depicted by so-called "envelope" diagrams in Figs. 1(a) and 1(b). In addition to the intratrimer exchange parameter J, additional intertrimer coupling pathways, denoted J_i $(i=0,1,2)$ [Fig. 1(d)], exist due to the existence of longer semicoordinate $Cu\cdots X$ interactions between trimers. Because of the competing exchange pathways between the trimers, an estimate of intertrimer exchange, denoted as J', as an average value of the J_i by inclusion of a mean-field correction to the susceptibility for an isolated trimer, may no longer be appropriate. For the antiferromagnetic trimer $(J<0)$ with a doublet ground state, the intertrimer coupling may lead to spin-frustration effects. The trimer chains studied by Grigereit *et al.* exhibited low-temperature behavior consistent with a doublet ground state for the individual trimers. However, in the intermediate-temperature regime, $\chi_M T$ showed behavior indicative of a more cooperative nature than expected for a simple trimer. This was modeled in an *ad hoc* fashion by applying a mean-field correction to the quartet state.

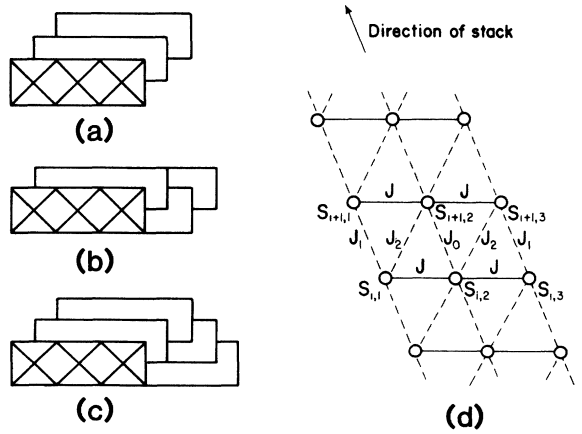

FIG. 1. (a)–(c) Stacking patterns for psuedoplanar $Cu_3X_8^{2-}$ trimers pertinent to this study. (d) Exchange pathways in trimer stacks. The solid lines and dashed lines represent intratrimer and intertrimer interactions, respectively.

Zaspel *et al.*[6] recently developed a high-temperature series-expansion model to calculate the zero-field susceptibility for the Heisenberg system corresponding to the exchange pathways shown in Fig. 1(d), in which the intertrimer exchange occurs as an expansion parameter. This method has been applied to estimate the intertrimer exchange coupling in (4-picolinium)$_2Cu_3Br_8$ (4-*PCB*) and (4-picolinium)$_2Cu_3Cl_8$ (4-PCC).[6] It was shown that the nearest-neighbor Heisenberg intratrimer exchange interaction, written in the form

$$\mathcal{H}=-2J(\mathbf{S}_1\cdot\mathbf{S}_2+\mathbf{S}_2\cdot\mathbf{S}_3)\ , \tag{1}$$

gave values for J/k of -30 K for 4-PCC and -100 K for 4-PCB. The antiferromagnetic coupling within the trimer results in an $S=\frac{1}{2}$ ground state. The low-temperature data were fitted to an expansion made in terms of the intertrimer exchange constants and the external field only. The surprising feature of the results was that, although the intertrimer exchange constants are all antiferromagnetic (with values of between 0.3 and 0.5 J), the low-temperature ordering of the trimers is ferromagnetic. Thus, both 4-PCC and 4-PCB belong to a rare but important class of pseudo-one-dimensional $S=\frac{1}{2}$ Heisenberg ferromagnets.

X-ray crystallographic determinations of the structures of 4-PCC, 4-PCB, and (1,1,4-trimethylpiperazinium)Cu_3Cl_8 (TMPC) are presented, along with the analysis of the magnetic susceptibility data for TMPC and details of the electron paramagnetic resonance (EPR) studies.

II. EXPERIMENT

A. Synthesis

The 4-picolinium halides were prepared by neutralizing 4-picoline with concentrated hydrogen halide solution, recrystallizing the product from water, and washing with acetone. The copper salts were crystallized from ~6M hydrogen halide solutions containing stoichiometric amounts of the appropriate 4-picolinium halide and copper (II) chloride dihydrate or copper (II) bromide. The preferred direction of crystal growth is parallel to the c axis of the unit cell. A cross section of a crystal taken perpendicular to the c axis generally has the shape of a parallelogram bounded by the (110), ($\bar{1}$10), (1$\bar{1}$0), ($\bar{1}\,\bar{1}$0) crystal planes. The chloride salt is a red-orange color when viewed along two directions of the crystal (one of which is the c axis) and a green-yellow color along the third. Thin sections of the bromide salt are purple. Both systems are pleochroic.

1,1,4-trimethylpiperazinium chloride was synthesized by reacting a 2:1 molar ratio of methyl chloride and 1,4-dimethylpiperazine in a Parr bomb for 24 h. Crystals of the title compound were grown by a temperature-gradient technique from a 6M HCl solution of 1,1,4-trimethylpiperazinium chloride and a large molar excess of copper (II) chloride dihydrate, maintained at a temperature of approximately 50°. These experimental conditions were chosen to minimize formation of the very insoluble tetrachlorocuprate (II) salts.

TABLE I. Crystal data.

Compound formula	4-PCC $C_{12}H_{16}Cl_8Cu_3N_2$	4-PCB $C_{12}H_{16}Br_8Cu_3N_2$	TMPC $C_7H_{18}Cl_8Cu_3N_2$
crystal class	monoclinic	monoclinic	monoclinic
space group	$C2/c$	$C2/c$	$P2_1/n$
a (Å)	24.578(5)	28.207(5)	7.227(1)
b (Å)	12.278(2)	12.779(2)	19.356(3)
c (Å)	7.106(1)	14.735(2)	13.421(2)
β (deg)	95.01(1)	116.71(1)	98.29(1)
V (Å^3)	2136.0(6)	4744(1)	1857.8(5)
Z	4	8	4
ρ (g/cm^3)	2.06	2.85	2.16
abs. coeff., μ (cm^{-1})	39.8	160.3	45.68
Transmission (min–max)	0.290–0.577	0.046–0.167	0.472–0.835
R	0.0345	0.0561	0.0374
R_w	0.0500	0.0500	0.0357

B. Crystal-structure determinations

Single-crystal x-ray-diffraction data were collected at Washington State University with a Syntex $P2_1$ automated four-circle diffractometer that has been upgraded to Nicolet R3m specifications.[16] Least-squares refinement of the angular settings of 25 well-centered high-angle reflections gave the cell parameters listed in Table I. Lp and crystal decay corrections were applied to the data, as was a numerical absorption correction. Crystal-structure solutions and refinements were accomplished using the SHELXTL package of programs.[17] Hydrogen atoms were included in the refinement and constrained to C-H and N-H distances of 0.96 Å and an idealized geometry. Data collection and final refinement parameters are listed in Table I, while a list of the atomic positions and equivalent isotropic thermal parameters may be found in Table II–IV. Details of the data collection and refinement procedures, as well as tables of observed and calculated structure factors, anisotropic thermal parameters, and hydrogen-atom positions have been placed in the supplementary material.

TABLE II. Atomic coordinates ($\times 10^4$) and equivalent isotropic thermal parameters (10^3Å^2) for 4-PCC.

Atom	x	y	z	U
Cu(1)	5000	756(1)	7500	28(1)
Cu(2)	3767(1)	782(1)	4994(1)	27(1)
Cl(1)	3271(1)	−508(1)	3345(1)	28(1)
Cl(2)	3202(1)	2114(1)	3946(1)	41(1)
Cl(3)	5582(1)	−521(1)	8882(1)	28(1)
Cl(4)	4421(1)	2033(1)	6178(1)	35(1)
N	2246(1)	813(2)	1361(4)	33(1)
C(1)	2012(1)	−112(3)	750(4)	35(1)
C(2)	1483(1)	−106(3)	−30(4)	37(1)
C(3)	1191(1)	862(3)	−215(4)	35(1)
C(31)	619(1)	916(4)	−1117(6)	64(2)
C(4)	1454(1)	1804(3)	436(4)	39(1)
C(5)	1983(1)	1764(3)	1247(4)	37(1)

C. Magnetic susceptibility measurements

Powder magnetic susceptibility data for TMPC were taken on a EG&G model 155 vibrating sample magnetometer at Montana State University in applied fields up to 5000 Oe from 4.2 to 200 K. No field dependence was found. The data, shown as points in Fig. 2, are plotted as

TABLE III. Atomic coordinates ($\times 10^4$) and equivalent isotropic thermal parameters (10^3 Å^2) for 4-PCB. The equivalent isotropic U is equal to one-third the trace of the orthogonalized U_{ij} tensor.

Atom	x	y	z	U
Cu(1)	0	1473(2)	2500	35(1)
Cu(2)	1268(1)	1480(2)	2543(1)	33(1)
Cu(3)	0	0	0	33(1)
Cu(4)	1254(1)	107(2)	−42(1)	31(1)
Br(1)	606(1)	168(1)	2430(1)	30(1)
Br(2)	597(1)	2780(1)	2429(1)	40(1)
Br(3)	1774(1)	163(1)	2210(1)	31(1)
Br(4)	1878(1)	2828(1)	2703(1)	42(1)
Br(5)	608(1)	−1255(1)	−82(1)	31(1)
Br(6)	569(1)	1353(1)	−127(1)	36(1)
Br(7)	1804(1)	−1252(1)	−144(1)	37(1)
Br(8)	1792(1)	1451(1)	−227(1)	38(1)
N(1)	2202(5)	5048(11)	320(8)	39(6)
C(11)	1958(6)	5962(15)	134(12)	47(9)
C(12)	1426(6)	6015(15)	−12(11)	45(8)
C(13)	1173(6)	5121(17)	63(11)	49(9)
C(14)	1456(7)	4171(15)	252(12)	52(9)
C(15)	1980(6)	4121(14)	398(11)	46(8)
C(16)	602(8)	5117(19)	−92(15)	102(14)
N(2)	2155(5)	3507(10)	−2369(9)	35(6)
C(21)	1944(7)	4373(12)	−2167(11)	43(8)
C(22)	1453(5)	4341(14)	−2261(11)	41(8)
C(23)	1168(5)	3480(12)	−2502(11)	27(7)
C(24)	1384(5)	2584(13)	−2664(11)	40(8)
C(25)	1889(7)	2611(14)	−2594(11)	54(9)
C(26)	638(6)	3396(16)	−2539(14)	75(11)

TABLE IV. Atomic coordinates ($\times 10^4$) and isotropic thermal parameters (10^3 Å^2) for trimethylpiperazinium octachlorotricuprate(II) (TMPZ). Equivalent isotropic U is defined as one third of the trace of the orthogonalized U_{ij} tensor.

Atom	x	y	z	U
Cu(1)	2529(1)	5363(1)	351(1)	26(1)
Cu(2)	5901(1)	3793(1)	1577(1)	25(1)
Cu(3)	998(1)	4501(1)	2266(1)	26(1)
Cl(1)	6286(1)	3574(1)	−107(1)	29(1)
Cl(2)	6679(1)	4921(1)	1175(1)	29(1)
Cl(3)	4820(1)	4216(1)	2951(1)	30(1)
Cl(4)	4932(1)	2710(1)	1852(1)	33(1)
Cl(5)	8374(1)	4352(1)	−1845(1)	31(1)
Cl(6)	8478(1)	5723(1)	−615(1)	28(1)
Cl(7)	10 508(1)	6506(1)	−2298(1)	36(1)
Cl(8)	9237(1)	5235(1)	−3845(1)	37(1)
N(1)	10 968(4)	8598(1)	−1047(2)	29(1)
N(2)	8803(4)	8057(1)	472(2)	32(1)
C(1)	9515(5)	9024(2)	−630(3)	33(1)
C(2)	8010(5)	8589(2)	−283(3)	38(1)
C(3)	10 295(5)	7643(2)	99(3)	37(1)
C(4)	11 769(5)	8100(2)	−244(3)	34(1)
C(5)	10 177(5)	8236(2)	−2011(3)	41(1)
C(6)	12 516(6)	9069(2)	−1291(3)	46(1)
C(7)	7307(6)	7599(2)	751(3)	52(1)

$\chi_m T/C$ versus T ($C=\mu_B^2 g^2 N_A/4k$). This plot shows a similar behavior to that of (4-picolinium)$_2$Cu$_3$Cl$_8$[3] in that the spins in the individual trimers are coupled antiferromagnetically to form spin-$\frac{1}{2}$ doublets below an intermediate-temperature region.

D. Electron paramagnetic resonance measurements

The electron paramagnetic resonance (EPR) measurements described in this paper were carried out at Montana State University at 9.3 GHz on a Varian E109 series with an Oxford Instruments "flowthrough" cryostat and temperature controller. Conventional EPR geometry was used, with the microwave magnetic field perpendicular to both the steady and modulated magnetic fields. The sample was placed in contact with a carbon-glass thermometer.

The EPR measurements were made in three mutually perpendicular planes of single-crystal samples of 4-PCC and TMPC. The three planes, designated Planes 1, 2, and 3 were, respectively, a (110) plane that is a plane parallel to a crystal face containing the z axis, the plane obtained from it by a rotation of 90° about the c axis, and the plane perpendicular to the c axis, which is the (001) plane. The spectra in two adjacent planes of the (110) set were compared in a 4-PCC sample, and found to be equivalent, which is consistent with crystallographic data. The measurements in 4-PCB were restricted to the (110) plane for the reason given below.

The temperature dependence of the EPR spectra were studied between 4 K and room temperature. Unfortunately, above about 60 K in 4-PCC and TMPC and at all temperatures in 4-PCB, complicated spectra from Cu(II) monomers were present in addition to the broad trimer spectrum, thus preventing good quantitative measurements of the latter. As a result, the analyses of the 4-PCC and TMPC samples were confined to the low-temperature region, where appreciable narrowing of the trimer spectrum allowed the use of much lower spectrometer sensitivities. In 4-PCB, there was no noticeable narrowing of the broader trimer spectrum in this material as the temperature was lowered. The additional structure in 4-PCC and TMPC has been attributed to the impurity $CuCl_2 \cdot 2H_2O$.[18] The source of the impurity spectrum in 4-PCB is currently unknown.

As a result of the impurity interference, the observations in 4-PCB were confined to low-temperature linewidth measurements and very rough g-value estimates in the (110) plane. In 4-PCC, measurements were made of the temperature dependence of the linewidth below 100 K, and of the 15-K spectrum in the three mutually perpendicular planes described above.

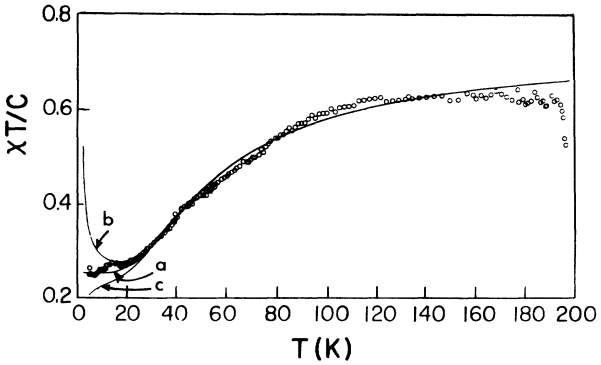

FIG. 2. Plot of the product $\chi_m T$ vs T for TMPC. Points are experimental results. The curve a is the calculated result of the noninteracting trimer model with $J/k=-33$ K. The curve b is the best-fit result of the simplest interacting trimer model with $J_0/k=J_1/k=-J_2/k=0.5$ K and $J/k=-33$ K, and curve c is the fit with $J_0/k=J_1/k=-J_2/k=-0.5$ K and $J/k=-33$ K.

III. STRUCTURAL RESULTS

All three structures consist of stacks of bibridged, quasiplanar $Cu_3X_8^{2-}$ trimers, as illustrated in Figs. 3 and 4. Due to the complexity of the stacking arrangement in 4-PCB, the structure contains two independent oligomers. Within each of the oligomers, the copper (II) ions attain a nearly planar four-coordinate geometry ($d_{Cu\text{-}Cl}=2.29$ Å, average; $d_{Cu\text{-}Br}=2.42$ Å, average). The organic cations hydrogen bond to terminal halides of the oligomers, with both ends of the oligomers capped by the picolinium cations in 4-PCC and 4-PCB (through bifurcated N—H · · · Cl hydrogen bonds), while, because of the difference in cation oligomer ratios and the availability of only a single proton available for hydrogen-bond formation, only one end of the TMPC oligomers are capped (via a normal N—H · · · Cl interaction). The aggregation of the oligomers occurs through the formation of longer, semicoordinate Cu · · · X bonds between adja-

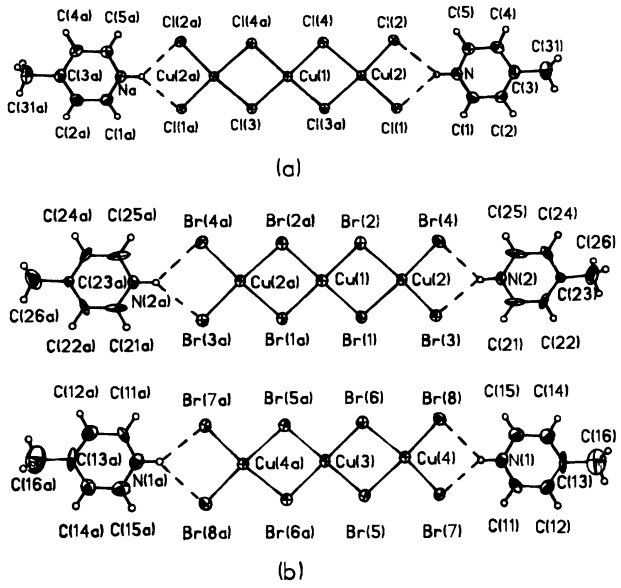

FIG. 3. (a) Illustration of the $Cu_3Cl_8^{2-}$ oligomer in 4-PCC and its hydrogen bonding with the 4-picolinium cations. (b) Illustration of the two $Cu_3Br_8^{2-}$ oligomers in 4-PCB and their hydrogen bonding with the 4-picolinium cations.

cent oligomers. In the two chloride salts, this leads to a stacking pattern of the type shown in Fig. 1(b). This stacking has been found previously for the trimeric oligomers in (N-methylpiperazinium)Cu_3Cl_8.[5] A new stacking pattern, depicted by the envelope diagram in Fig. 1(c), is exhibited by 4-PCB. Relevant bond distances and angles for the oligomers are given in Table V.

The $Cu_3X_8^{2-}$ oligomers all show deviations from idealized D_{2h} symmetry. These deviations can be attributed to the influence of the hydrogen bonding with the cations and to the semicoordinate bond formation between oligomers. The latter effect shows up in several ways. The translations associated with the formation of the semicoordinate bonds reduces the symmetry to, at most, C_2 or C_i. Next, it is observed that the halide ions involved in two semicoordinate bonds remain roughly equidistant between adjacent oligomers. However, when a terminal halide forms only one semicoordinate bond, the bond is shorter than normal and a nonplanarity is imposed upon the oligomers. The distortions caused by the hydrogen bonding are due to the asymmetric displacement of the cations about the oligomers. In 4-PCC and 4-PCB, this arises from the noncoplanarity of the oligomers and the cations. For TMPZ, the 1:1 oligomer-to-cation ratio forces a further reduction of the oligomer symmetry to merely C_1 (see Fig. 4). The net result is that the central Cu atoms attain a 4+2 coordination in which both semicoordinate bonds are equal (or nearly equal, for TMPZ), while the terminal Cu atoms may be better described as having a 4+1+1 geometry in which one semicoordinate bond is 0.5–0.7 Å longer than the other. Further

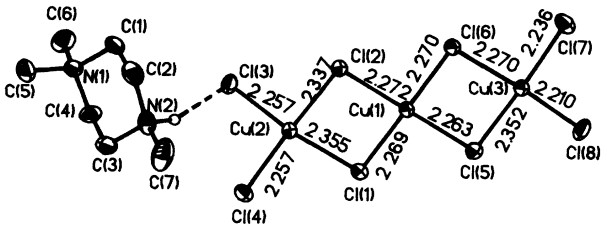

FIG. 4. Thermal ellipsoid plot of the formula unit of TMPC.

analysis of the observed distortions has been made.[11]

The magnetic coupling values for the various intertrimer exchange pathways (Fig. 1) are strongly dependent upon the nature of these distortions, in a manner that is not easily quantified. The oligomer stacks propagate parallel to the c axis for 4-PCC and 4-PCB, with the projection of the Cu-Cu axes onto the bc plane essentially parallel to the b axis. The angle between the normal to the oligomer planes and the c axis is 28° (4-PCC) or 23° (4-PCB). Neighboring stacks are related by translation symmetry, and thus are magnetically equivalent. For TMPZ, the stacks occur parallel to the a axis, and the Cu-Cu direction makes an angle of 61° with respect to the b axis. Neighboring stacks are related by nontranslational symmetry elements and so are magnetically inequivalent.

Structurally, the important feature of this study is this new stacking pattern[19] exhibited by 4-PCB. The set of the patterns in Fig. 1 has an intriguing property, in that a strong analogy can be seen with the ground states of the next-nearest-neighbor Ising model.[20] Here competing nearest- and next-nearest-neighbor interactions can lead to ferromagnetic ($\uparrow\uparrow\uparrow\uparrow\cdots$), antiferromagnetic ($\uparrow\downarrow\uparrow\downarrow\cdots$), or mixed or competition ($\uparrow\uparrow\downarrow\downarrow\cdots$) states. The polytypism exhibited in the stacking patterns for the psuedoplanar $Cu_nX_{2n}L_2$ oligomers is too complex to be described by an Ising model, since, in general, the relationship between repeating units must be specified by translations in one of four directions. We have been able to show that the polytypism can be modeled by a simple one-dimensional Hamiltonian, that of the XY model with cubic anisotropy.[21] This model predicts the existence of the above three phases, two additional observed stacking patterns in $(Et_2NH_2)_2Cu_3Br_8\cdot CuBr_2$,[22] and (4,4′-dimethyl-2,2′-dipyridine)Cu_2Cl_4,[21,23] as well as a number of currently unknown competition phases. A preliminary report has been given.[21(a)]

IV. MAGNETIC CALCULATIONS

The calculation of susceptibility corresponding to the interaction pathways in these stacked trimers may be carried out by the high-temperature series expansion of Zaspel *et al.* for the Heisenberg model with intertrimer exchange as an expansion parameter.[6] The pathways are defined in Fig. 1(d) and lead to the Hamiltonian

$$\mathcal{H}=\sum_{i=1}^{\infty}[-2J(\mathbf{S}_{i,1}\cdot\mathbf{S}_{i,2}+\mathbf{S}_{i,2}\cdot\mathbf{S}_{i,3})-2J_0(\mathbf{S}_{i,2}\cdot\mathbf{S}_{i+1,2})-2J_1(\mathbf{S}_{i,1}\cdot\mathbf{S}_{i+1,1}+\mathbf{S}_{i,3}\cdot\mathbf{S}_{i+1,3})-2J_2(\mathbf{S}_{i,1}\cdot\mathbf{S}_{i+1,2}+\mathbf{S}_{i,2}\cdot\mathbf{S}_{i+1,3})]\ . \quad (2)$$

TABLE V. Selected bond distances (Å) and angles (deg).

	4-PCC	Trimer *A*		4-PCB	Trimers *B*
		Central Cu atoms			
Cu(1)-Cl(3)	2.286(1)	Cu(1)-Br(1)	2.423(3)	Cu(3)-Br(5)	2.381(3)
Cu(1)-Cl(4)	2.265(1)	Cu(1)-Br(2)	2.407(3)	Cu(3)-Br(6)	2.423(2)
Cu(1)-Cl(3′)	2.063(1)	Cu(1)-Br(5)	3.197(2)	Cu(3)-Br(1′)	3.207(2)
		Terminal Cu atoms			
Cu(2)-Cl(1)	2.264(1)	Cu(2)-Br(1)	2.459(3)	Cu(4)-Br(5)	2.501(2)
Cu(2)-Cl(2)	2.231(1)	Cu(2)-Br(2)	2.468(3)	Cu(4)-Br(6)	2.464(3)
Cu(2)-Cl(3)	2.351(1)	Cu(2)-Br(3)	2.396(3)	Cu(4)-Br(7)	2.378(3)
Cu(2)-Cl(4)	2.327(1)	Cu(2)-Br(4)	2.371(3)	Cu(4)-Br(8)	2.388(3)
Cu(2)-Cl(1′)	2.790(1)	Cu(2)-Br(7′)	3.057(3)	Cu(4)-Br(3′)	2.964(2)
Cu(2)-Cl(3′)	3.319(1)	Cu(2)-Br(6′)	3.525(3)	Cu(4)-Br(1′)	3.350(3)
		Central Cu atoms			
Cl(3)-Cu(1)-Cl(4)	179.0(1)	Br(1)-Cu(1)-Br(2)	87.5(1)	Br(5)-Cu(3)-Br(6)	87.7(1)
Cl(3)-Cu(1)-Cl(3′)	93.4(1)	Br(1)-Cu(1)-Br(1′)	93.0(1)	Br(5)-Cu(3)-Br(6′)	92.3(1)
Cl(3)-Cu(1)-Cl(4′)	87.1(1)	Br(1)-Cu(1)-Br(2′)	179.5(1)		
Cl(4)-Cu(1)-Cl(4′)	92.4(1)	Br(2)-Cu(1)-Br(2′)	92.1(1)		
		Terminal Cu atoms			
Cl(1)-Cu(2)-Cl(2)	92.8(1)	Br(1)-Cu(3)-Br(2)	85.3(1)	Br(5)-Cu(4)-Br(6)	84.4(1)
Cl(1)-Cu(2)-Cl(4)	166.8(1)	Br(1)-Cu(2)-Br(3)	90.6(1)	Br(5)-Cu(4)-Br(7)	88.8(1)
Cl(1)-Cu(2)-Cl(3)	91.1(1)	Br(1)-Cu(3)-Br(4)	175.9(1)	Br(5)-Cu(4)-Br(8)	172.6(1)
Cl(2)-Cu(2)-Cl(4)	91.6(1)	Br(2)-Cu(2)-Br(3)	165.6(1)	Br(6)-Cu(4)-Br(7)	171.1(1)
Cl(2)-Cu(2)-Cl(3)	175.6(1)	Br(2)-Cu(2)-Br(4)	91.0(1)	Br(6)-Cu(4)-Br(8)	93.1(1)
Cl(4)-Cu(2)-Cl(3)	84.2(1)	Br(3)-Cu(2)-Br(4)	93.3(1)	Br(7)-Cu(4)-Br(8)	93.0(1)
		Bridging angles			
Cu(1)-Cl(3)-Cu(2)	93.5(1)	Cu(1)-Br(1)-Cu(2)	93.2(1)	Cu(3)-Br(5)-Cu(4)	93.7(1)
Cu(1)-Cl(4)-Cu(2)	94.7(1)	Cu(1)-Br(2)-Cu(2)	93.4(1)	Cu(3)-Br(6)-Cu(4)	93.8(1)

	TMPC		
	Central Cu atoms		
Cu(1)-Cl(1)	2.269(1)	Cu(1)-Cl(6)	2.271(1)
Cu(1)-Cl(2)	2.273(1)	Cu(1)-Cl(2′)	3.162(1)
Cu(1)-Cl(5)	2.263(1)	Cu(1)-Cl(6′)	3.107(1)
	Terminal Cu atoms		
Cu(2)-Cl(1)	2.355(1)	Cu(3)-Cl(5)	2.352(1)
Cu(2)-Cl(2)	2.377(1)	Cu(3)-Cl(6)	2.341(1)
Cu(2)-Cl(3)	2.257(1)	Cu(3)-Cl(7)	2.237(1)
Cu(2)-Cl(4)	2.257(1)	Cu(3)-Cl(8)	2.210(1)
Cu(2)-Cl(7′)	2.700(1)	Cu(3)-Cl(3′)	2.837(1)
Cu(2)-Cl(6′)	3.374(1)	Cu(3)-Cl(2′)	3.353(1)
	Central Cu atoms		
Cl-Cu(1)-Cl(1)	86.6(1)	Cl(2)-Cu(1)-Cl(5)	177.8(1)
Cl-Cu(1)-Cl(2)	94.0(1)	Cl(2)-Cu(1)-Cl(6)	92.5(1)
Cl-Cu(1)-Cl(6)	176.6(1)	Cl(5)-Cu(1)-Cl(6)	87.0(1)
	Terminal Cu atoms		
Cl(1)-Cu(2)-Cl(2)	83.2(1)	Cl(5)-Cu(3)-Cl(6)	83.4(1)
Cl(1)-Cu(2)-Cl(3)	162.2(1)	Cl(5)-Cu(3)-Cl(7)	159.9(1)
Cl(1)-Cu(2)-Cl(4)	94.1(1)	Cl(5)-Cu(3)-Cl(8)	93.2(1)
Cl(2)-Cu(2)-Cl(3)	88.4(1)	Cu(6)-Cu(3)-Cl(7)	90.1(1)
Cl(2)-Cu(2)-Cl(4)	174.9(1)	Cu(6)-Cu(3)-Cl(8)	174.5(1)
Cl(3)-Cu(2)-Cl(4)	92.9(1)	Cl(7)-Cu(3)-Cl(8)	94.5(1)
	Bridging angles		
Cu(1)-Cl(2)-Cu(2)	94.7(1)	Cu(1)-Cl(5)-Cu(3)	94.2(1)
Cu(1)-Cl(1)-Cu(2)	94.3(1)	Cu(1)-Cl(6)-Cu(3)	94.3(1)

The calculation yields the expression

$$\frac{\chi_m T}{C}=\frac{\chi_0 T}{C}+\frac{2}{T}\{2J_1(\tfrac{1}{4}+C_1^z+C_2^z)^2+2J_2[\tfrac{1}{16}+\tfrac{3}{4}C_1^z+\tfrac{1}{4}C_2^z+2(C_1^z)^2+2C_1^zC_2^z]+J_0(2C_1^z+\tfrac{1}{4})^2\}$$
$$+\frac{2}{T^2}\left[(\tfrac{1}{4}+C_1^z+C_2^z)^2\frac{J_1^2}{2}+\frac{J_2^2}{4}+4J_1J_2C_1^z+2J_1^2C_2^z+(2C_1^z+\tfrac{1}{4})^2(2J_0J_2C_1^z+J_2^2C_2^z+J_0^2/4)\right.$$
$$\left.+(2C_1^z+\tfrac{1}{4})(\tfrac{1}{4}+C_1^z+C_2^z)(4J_0J_1C_1^z+2J_1J_2C_2^z+\tfrac{1}{2}J_1J_2+\tfrac{1}{2}J_0J_2+2J_2^2C_1^z)\right]$$
$$+\frac{J\chi_0}{12C}\frac{(J_1J_2+J_0J_2-J_0^2-J_1^2-J_2^2)}{T^2(1+2e^{\beta J}+e^{-2\beta J})}\ , \tag{3}$$

where the first term is the isolated trimer molar susceptibility:

$$\frac{\chi_0 T}{C}=\frac{10+e^{-\beta J}+e^{-3\beta J}}{4(2+e^{-\beta J}+e^{-3\beta J})}\ . \tag{4}$$

Here C_1^z and C_2^z are the nearest- and next-nearest-neighbor zz spin correlation functions, with

$$C_2^z=\frac{2e^{\beta J}-3+e^{-2\beta J}}{4(2e^{\beta J}+1+e^{-2\beta J})}\ , \tag{5}$$

and C_1^z was obtained from the fluctuation-dissipation theorem, and

$$\frac{\chi_0 T}{C}=\tfrac{3}{2}+4C_1^z+2C_2^z\ , \tag{6}$$

where

$$C=\frac{\mu_B^2 g^2 N_A}{k}\ . \tag{7}$$

This expression has been used to fit the data[24] for 4-PCC and 4-PCB with the results $J/k=-31.0$ and -100 K, respectively. The expression was also applied to some of the data reported by Grigereit *et al.*[5]

The behavior of this model will depend upon the sign combinations (and magnitudes) of the three intertrimer interaction constants J_0, J_1, and J_2. Table VI lists the possible net intrastack interactions for the situation when $|J_0|=|J_1|=|J_2|$. It is seen that four combinations produce a net ferromagnetic coupling, while four lead to an antiferromagnetic behavior. Spin-frustration effects are avoided for only two of the sign combinations (entires 2 and 7 in Table VI), while the other sign combinations lead to a mild (entries 3 and 6) or strong degree of spin frustration.

TABLE VI. Effective intertrimer exchange coupling J_{eff} for the Zaspel model for sign permutations of J_i parameters with $|J_0|=|J_1|=|J_2|$.

J_0	J_1	J_2	J_{eff}
+	+	+	$\frac{1}{5}J_i$
+	+	−	J_i
+	−	+	$-\frac{3}{5}J_i$
+	−	−	$\frac{1}{3}J_i$
−	+	+	$-\frac{1}{5}J_i$
−	+	−	$\frac{3}{5}J_i$
−	−	+	$-J_i$
−	−	−	$-\frac{1}{5}J_i$

First, we considered the simplest isolated trimer model in which all of the intertrimer exchange coupling constants are zero. The optimum value of the intratrimer exchange constant $J/k=-33$ K was found from the fit to the data in the temperature range from 200 to 25 K (see curve *a* in Fig. 2). The apparent difference between the calculation and the data below 30 K clearly indicates an existence of intertrimer and/or interstack interactions. However, agreement is reasonably good in the high-temperature regime, indicating the absence of any substantial amount of spin frustration. The small deviations between experiment and theory in the 50–120-K region do not rule out the presence of a small amount of frustration. Nevertheless, in this study, only the two combinations of signs for the intertrimer exchange were considered: (i) $J_0>0$, $J_1>0$, and $J_2<0$; (ii) $J_0<0$, $J_1<0$, and $J_2>0$. Curve *b* in Fig. 2 is the result of the calculation with $J_0/k=J_1/k=-J_2/k=0.5$ K. This leads to a ferromagnetic ground state for the stack. Curve *c* is obtained for $J_0/k=J_1/k=-J_2/k=-0.5$ K and corresponds to an antiferromagnetic spin arrangement for the stack. Curve *b* reproduces the data in the regime 15 K $<T<$ 25 K, but the $\chi_m T$ data fail to continue to rise at lower temperature. This is likely due to interstack interactions.

V. EPR RESULTS: $S=\frac{1}{2}$ SPECTRUM OF 4-PCC

The 9.3-GHz EPR spectra of 4-PCC were measured at several temperatures between 4 and 160 K for two orientations in the (110) plane. For the orientation giving the narrowest lines, a single peak was observed at all temperatures, which narrowed substantially as the temperature decreased. The measured peak-to-peak widths at 14, 31, 53, and 73 K were approximately 70, 190, 435, and 510 G, respectively. While linear dependencies of the linewidth on temperature, which are associated with the modulation of the antisymmetric exchange interaction by a single-phonon process,[25] have often been observed in materials of the type,[26] this is clearly not the case for 4-PCC. Here the temperature dependence between 4 and 53 K is approximately quadratic, while above 80 K there is very little further change of linewidth. In contrast with the field parallel to the *c* axis, fine structure is resolved in this case as the temperature is lowered (Fig. 5).

The angular variation of the EPR spectrum of 4-PCC near 15 K in Plane 2 showed a doubling of unknown origin of the $S=\frac{1}{2}$ trimer line over a range of orientations from 15° to 45° from the *c* axis in both directions. Neglecting the line doubling observed in Plane 2, the

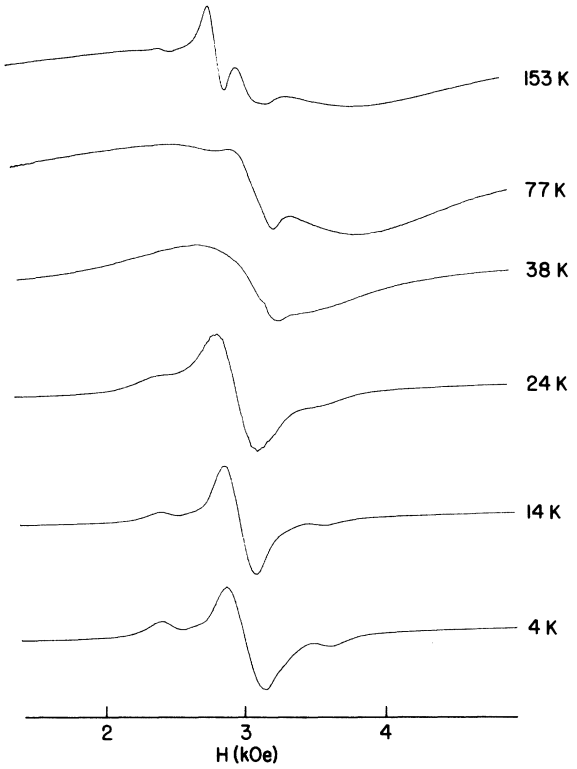

FIG. 5. EPR spectra of 4-PCC at 9.3 GHz are shown at various temperatures with the external magnetic field parallel to the the crystallographic c axis. Weak lines, probably associated with an $S=\frac{3}{2}$ trimer state, may be seen in the 4-, 14-, and 24-K spectra.

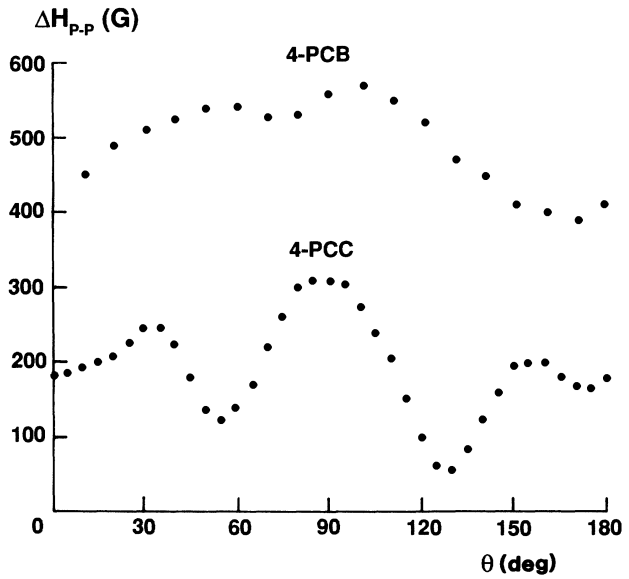

FIG. 6. The peak-to-peak linewidths at 9.3 GHz measured in the (110) plane of 4-PCC at 17 K and 4-PCB at 4 K are plotted as functions of the angle of rotation θ from the c axis. In 4-PCC, the z direction is at $\theta=(26\pm2)°$.

principal g values for the exchange-coupled EPR spectra for 4-PCC at 15 K were estimated by means of a standard analysis,[27] to be as follows:

$$g_z=2.264\pm0.001\ ,$$
$$g_x=2.047\pm0.001\ , \quad (8)$$
$$g_y=2.068\pm0.002\ ,$$

where the y direction is parallel to the crystallographic b axis, and the z and x directions are in the ac plane with the former making an angle of $(26\pm2)°$ with the c axis. This angle is in approximate agreement with the angle of 27.9° between the normal to the trimer plane and the c axis obtained from the x-ray data, indicating that the z direction makes an angle of about 121° with the crystallographic a axis.

In 4-PCC, the measured linewidths at low temperatures varied from sample to sample by as much as a factor of 2. Measurements at 17 K in a (110) plane of the sample giving the narrowest lines are shown in Fig. 6. Choosing the c axis as the origin, maxima in the peak-to-peak linewidth of approximately 250, 310, and 205 G were observed near the angles 30°, 90°, and 160°, respectively, while minima of 125, 60, and 165 G were observed at 55°, 130°, and 175°. The linewidth variations show a close resemblance to those observed in the ac planes of systems as diverse as $CuTiF_6\cdot6H_2O$ (Ref. 28) and $[(CH_3)_3NH]CuCl_3\cdot2H_2O$.[29] Shown in Fig. 6 is the corresponding linewidth variation in 4-PCB at 4 K. In this case, much broader lines have peak-to-peak widths varying from 390 to 570 G. Because of the presence of the impurity spectrum, good g-value measurements could not be obtained for 4-PCB. Approximate extrema in the (110) plane were $g_{max}\approx2.09$ and $g_{min}\approx2.04$, with the maximum occurring at $\theta\approx30°$, which may be compared with the value of $(26\pm2)°$ obtained in 4-PCC.

VI. EPR RESULTS: $S=\frac{3}{2}$ SPECTRUM OF 4-PCC

The weak outer fine-structure lines of an $S=\frac{3}{2}$ spectrum may be seen in the 4-, 14-, and 24-K spectra of Fig. 5 for 4-PCC. This spectrum could be observed only in a range of about 30° on either side of the c axis in both planes 1 and 2. The relative intensity of either line was about 5% that of the main $S=\frac{1}{2}$ spectrum, and increased slightly as the temperature was reduced from 20 to 4 K. In the (110) plane (plane 1), the maximum in the fine-structure splitting was close to the c axis, while the extrema of the upper and lower fine-structure lines occurred about 6° on either side of the c axis, indicating that this direction was not associated with a g-value extremum. Thus, the principal axes of the g and D tensors are not equivalent for the $S=\frac{3}{2}$ spectrum. In plane 2, the extrema of both fine-structure lines were found to be in the c direction.

In order to better resolve the outer lines of the $S=\frac{3}{2}$ fine-structure spectrum, computer simulations were used to subtract the dominant $S=\frac{1}{2}$ line from the overall spectrum. (This procedure also removed the central line of

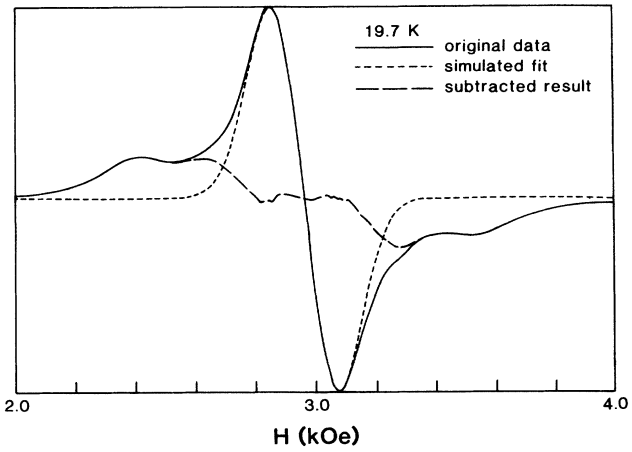

FIG. 7. The EPR spectrum in the *c* direction is shown at 19.7 K. The solid line is the observed spectrum, while the dashed lines are the simulated fit of the central $S=\frac{1}{2}$ line and the result of subtracting it from the observed spectrum.

the $S=\frac{3}{2}$ spectrum.) This was done by fitting the central part of the observed spectrum to a Lorentzian curve. The criterion used to obtain the best fit was the production of the flattest region at the center of the $S=\frac{1}{2}$ line after subtraction. Figures 7 and 8 show the measured spectrum, the simulated fit of the $S=\frac{1}{2}$ line, and the subtracted result at 19.7 and 3.7 K, respectively. In both cases the magnetic field was parallel to the *c* axis, as in Fig. 5.

The most striking aspect of the subtracted result of both Figs. 7 and 8 is the presence of two distinct sets of lines that could each correspond to the outer transitions of an $S=\frac{3}{2}$ manifold. The double set of spectra could be due to twinning or to a lower-symmetry component in the crystal structure. If the outermost pair of lines are assumed to fit a spin Hamiltonian of the form

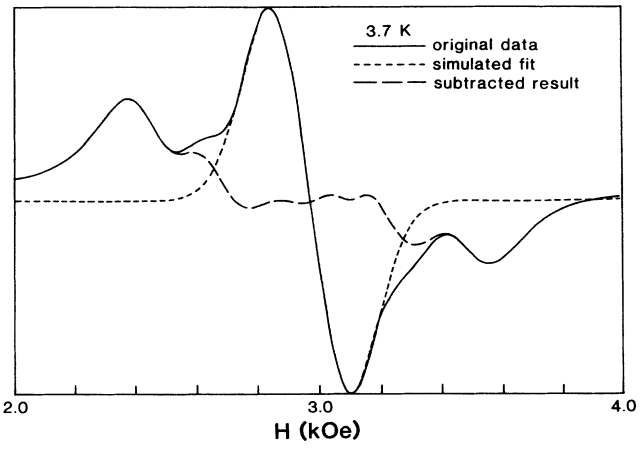

FIG. 8. The EPR spectrum in the *c* direction is shown at 3.7 K. The solid line is the observed spectrum, while the dashed lines are the simulated fit of the central $S=\frac{1}{2}$ line and the result of subtracting it from the observed spectrum.

$$\mathcal{H}=g_C\mu_B HS_z+DS_z^2\ , \tag{9}$$

then the values $g_C=2.23\pm0.01$ and $|D|=(0.026\pm0.001)$ cm^{-1} are obtained for the 3.7-K data.

A disturbing feature of the fine-structure spectra was the increase in their relative intensities with respect to the intense $S=\frac{1}{2}$ spectrum as the temperature was lowered. This effect was most pronounced in the outermost pair of lines, their relative intensity almost doubling as the temperature was decreased from 19.7 to 3.7 K.

To significantly populate the $S=\frac{3}{2}$ manifold at temperatures below 10 K would require major deviations from the Heisenberg Hamiltonian of Eq. (1) where $J/k=-30$ K for 4-PCC, suggesting that the $S=\frac{3}{2}$ spectra could be associated with crystalline imperfections, such as stacking faults (see Discussion).

VII. EPR RESULTS: TMPC

The anisotropic spectra observed at room temperature for TMPC were similar to those reported in other materials of this type, which have been attributed to the impurity $CuCl_2\cdot2H_2O$.[18] On cooling the sample, an additional broader spectrum appeared below 50 K, narrowing to become the dominant spectrum at liquid-helium temperatures. As in the case of 4-PCC, this spectrum is associated with an $S=\frac{1}{2}$ trimer ground state. The extrema of this spectrum were found to be $g_{max}=2.259\pm0.005$ and $g_{min}=2.055\pm0.003$, with g_{max} in a direction approximately parallel to the crystallographic *c* axis. Peak-to-peak linewidths of between 60 and 260 G were obtained for the derivative signal, with the latter corresponding to g_{max}. An unresolved doubling of the line was observed for a range of orientations of about 40° in plane 3, which is unlike the results of 4-PCC, where no doubling was observed in that plane. Using the limited information currently available, the anisotropy of the sample can be represented by the approximate values $g_{\parallel}\cong2.26$ and $g_{\perp}\cong2.06$, with the former value in the direction of the crystallographic *c* axis. These values are similar to the more precise values obtained for 4-PCC, which are given in Eq. (8).

VIII. DISCUSSION

The structural parameters (Cu coordination geometry, Cu-*X* distances, Cu-*X*-Cu angles) for the three new $A_2Cu_3X_8$ salts reported here are in accord with those for previously studied systems.[5] In particular, the near planarity of the trimeric species ensures that the unpaired electrons lie in $d_{x^2-y^2}$-like orbitals on the individual copper atoms. The values observed for the Cu-*X*-Cu angles are in the range normally associated with antiferromagnetic exchange coupling, which arises due to overlap of the magnetic orbitals at the bridging halide ions. The magnetic susceptibility and EPR measurements confirm that the coupling within the trimers is reasonably strong and antiferromagnetic, leaving a spin doublet as a ground state. The values of the intratrimer coupling found for 4-PCC and TMPC ($-31,-33$ K) are consistent with those found in previously studied $Cu_3Cl_8^{2-}$, confirming

that magnetostructural correlations allow exchange parameters to be transferred between structurally related systems. The coupling is substantially stronger in 4-PCB (−100 K). This agrees with the general trend that the antiferromagnetic contribution to the exchange coupling is substantially larger in copper (II) bromides than the corresponding chlorides[30] due to the existence of lower-lying ligand-to-metal charge-transfer electronic transitions.

The intertrimer interactions with the stacks are found to be weak, and antiferomagnetic in nature. Within the Zaspel model,[6] deviations observed in the high-temperature regime can be accounted for by the presence of spin-frustration effects due to competing intertrimer coupling constants, as found in 4-PCC.[24] In TMPC, the absence of substantial spin frustration in the high-temperature region and the incipient rise of χT below 30 K leads to the assignment $J_0, J_1 > 0$ and $J_2 < 0$.

The EPR data are essentially consistent with both the magnetic susceptibility and x-ray crystallographic interpretations; however, as is often the case, additional fine features are observed that indicate that the interpretation should be modified. The dominant $S = \frac{1}{2}$ EPR spectrum agrees with the $S = \frac{1}{2}$ ground state used in the susceptibility analysis, while the equivalence of the EPR spectra obtained in two adjacent (110) planes of a 4-PCC crystal is consistent with the crystallographic structure. Furthermore, as noted in the text, the angle obtained by EPR between the z direction of the g tensor and the crystallographic c axis for 4-PCC agrees with that between the normal to the trimer plane and the c axis obtained from the x-ray data. On the other hand, a splitting of the low-temperature $S = \frac{1}{2}$ spectra is observed clearly in both 4-PCC and TMPC for a small range of orientations. This may be due the existence of two inequivalent trimer arrangements as a result of an undetected structural phase transition. The apparent $S = \frac{3}{2}$ spectra observed below 30 K in 4-PCC could arise from a number of sources. Stacking faults could lead to deformation of $Cu_3Cl_8^{2-}$ trimers at the fault sites such that a ferromagnetic coupling is induced. Alternatively, stacking faults could lead to the presence of truncated stacks of three trimers (or a greater odd number). The ferromagnetic coupling of the ground-state doublets of individual trimers would then give rise to the observed quartet state.

The stacking of $Cu_3X_8^{2-}$ trimeric units in 4-PCB represents a new polytypic structure for the $A_2Cu_nX_{2n+2}$ series of copper(II) halide salts. The ramifications of this stacking pattern, with respect to developing a phenomonological model to account for observed patterns and to predict new patterns, is being developed in other publications.[21]

Supplementary material available. The following tables are available from R. D. Willett for the compounds 4-PCC, 4-PCB, and TMPC: refinement parameters (six pages), complete listing of distances and angles (six pages), tables of anisotropic thermal parameters and hydrogen-atom coordinates (three pages), and observed and calculated structure factors (65 pages).

ACKNOWLEDGMENTS

This work was supported by the National Science Foundation under Grant Nos. DMR 87-02933 and DMR 88-03382. The x-ray-diffraction laboratory was established through funds contributed by The Boeing Company and the National Science Foundation (Grant No. CHE-8408407).

*Present address: Department of Physics, Western Montana College, Dillon, Montana 59725.

†Present address: Institut für Physik, Universität Mainz, Mainz, West Germany.

[1]R. D. Willett, T. Grigereit, K. E. Halvorson, and B. Scott, Proc. Indian Acad. Sci. **98**, 147 (1987).

[2]M. R. Bond and R. D. Willett, Inorg. Chem. **28**, 3267 (1989).

[3]T. Grigereit and R. D. Willett, J. Appl. Phys. **61**, 3292 (1987).

[4]S. O'Brien, R. M. Gaura, C. P. Landee, B. L. Ramakrishna, and R. D. Willett, Inorg. Chim. Acta **141**, 83 (1987).

[5]T. E. Grigereit, B. L. Ramakrishna, H. Place, R. D. Willett, G. C. Pellacani, T. Manfredini, L. Menabue, A. Bonamartini-Corradi, and L. P. Battaglia, Inorg. Chem. **26**, 2235 (1987), and references therein.

[6]C. E. Zaspel, G. V. Rubenacker, S. L. Hutton, J. E. Drumheller, R. S. Rubins, R. D. Willett, and M. R. Bond, J. Appl. Phys. **63**, 3028 (1988).

[7]G. V. Rubenacker, J. E. Drumheller, K. Emerson, and R. D. Willett, J. Magn. Magn. Mater. **54**, 1485 (1986); K. E. Halvorson, T. Grigereit, and R. D. Willett, Inorg. Chem. **26**, 1716 (1987).

[8]G. V. Rubenacker, J. E. Drumheller, and K. Emerson, J. Magn. Magn. Mater. **61**, L1 (1986).

[9]P. Zhou, J. E. Drumheller, G. V. Rubenacker, M. R. Bond, and R. D. Willett, J. Phys. Colloq. **49**, C8-1478 (1988).

[10]C. E. Zaspel, P. Zhou, and J. E. Drumheller, J. Magn. Magn. Mater. **79**, 303 (1989).

[11]M. Bond, Ph.D. thesis, Washington State University, 1990.

[12]J. C. Livermore, R. D. Willett, R. M. Gaura, and C. P. Landee, Inorg. Chem. **21**, 1403 (1982).

[13]C. Weng, doctoral dissertation, Carnegie-Mellon University, 1968.

[14]H. Akagi and N. Uryu, Phys. Lett. **86A**, 248 (1981).

[15]C. P. Landee, A. Djili, D. F. Mudgett, M. Newhall, H. Place, B. Scott, and R. D. Willett, Inorg. Chem. **27**, 620 (1988).

[16]C. F. Campana, D. F. Shepard, and W. M. Litchman, Inorg. Chem. **20**, 4039 (1981).

[17]G. M. Sheldrick, SHELXTL, Revision 4.1 (Nicolet Instrument Corp., Madison, WI, 1985). Scattering factors from *International Tables for X-ray Crystallography* (Kynock, Birmingham, 1974), Vol. IV (present distributor Reidel, Dordrecht, The Netherlands).

[18]B. Scott, U. Geiser, R. D. Willett, B. Patyal, C. P. Landee, R. E. Greeney, T. Manfredini, G. C. Pellacani, A. Bonamartini-Corradi, and L. P. Battaglia, Inorg. Chem. **27**, 2454 (1988).

[19]U. Geiser, R. D. Willett, M. Lindbeck, and K. Emerson, J.

Am. Chem. Soc. **108**, 1173 (1986).
[20]P. Bak and J. von Boehm, Phys. Rev. B **21**, 5297 (1980).
[21](a) R. D. Willett, M. R. Bond, and G. Pon, Inorg. Chem. **29**, 4160 (1990); (b) R. D. Willett, J. Phys. Condens. Matter (to be published).
[22]R. Fletcher, J. Livermore, J. J. Hansen, and R. D. Willett, Inorg. Chem. **22**, 330 (1983).
[23]G. Pon and R. D. Willett (unpublished).
[24]K. Schittkowski, *NLPQL: A FORTRAN Subroutine Solving Constrained Nonlinear Programming Problems,* edited by L. Clyde Monma [Ann. Operations Res. **5**, 485 (1986)].
[25]T. G. Castner, Jr. and M. S. Seehra, Phys. Rev. B **4**, 38 (1971).
[26]T. M. Kite, J. E. Drumheller, and K. Emerson, J. Magn. Reson. **48**, 20 (1983); R. D. Willett, R. J. Wong, and M. Numata, Inorg. Chem. **22**, 3189 (1983).
[27]C. P. Poole, Jr. and H. A. Farach, *Theory of Magnetic Resonance,* 2nd ed. (Wiley, New York, 1987), pp. 59–65.
[28]R. S. Rubins, D. K. De, and T. D. Black, J. Chem. Phys. **75**, 128 (1971).
[29]M. B. Ritter, J. E. Drumheller, T. M. Kite, L. O. Snively, and K. Emerson, Phys. Rev. B **28**, 4949 (1983).
[30]B. Scott and R. D. Willett, J. Appl. Phys. **61**, 3289 (1987).